JPNT 8(4), 165-173 (2019)
https://doi.org/10.11003/JPNT.2019.8.4.165

JPNT Journal of Positioning, Navigation, and Timing

Performance of Interference Mitigation with Different Wavelets in Global Positioning Systems

Bo-Seok Seo[1†], Kwi-Woo Park[2], Chansik Park[1]

[1]Department of Electronics Engineering, Chungbuk National University, Cheongju 28644, Korea
[2]R&D Center of NavCours Co. Ltd., Daejeon 34014, Korea

ABSTRACT

In this paper, we apply a discrete wavelet packet transform (DWPT) to reduce the influence of interference in global positioning system (GPS) signals and compare the interference mitigation performance of various wavelets. By applying DWPT to the received signal, we can gradually divide the received signal band into low-pass and high-pass bands. After calculating the average power for the separate bands, we can determine whether there is interference by comparing the value with the given threshold. For a band that includes interference, we can reconstruct the whole band signal using inverse DWPT (IDWPT) after applying a nulling method that sets all of the wavelet coefficients to 0. The reconstructed signals are correlated with the pseudorandom noise (PRN) codes to acquire GPS signals. The performance evaluation is based on the number of satellite signals whose peak ratio (defined as the ratio of the first and second correlation peak values in the acquisition stage) exceeds the threshold. In this paper, we compare and evaluate the performance of 6 wavelets including Haar, Daubechies, Symlets, Coiflets, Biorthogonal Splines, and Discrete Meyer.

Keywords: GPS, GNSS, interference detection and mitigation, discrete wavelet packet transform

1. INTRODUCTION

Radio jamming is the deliberate jamming, blocking or interference of communication systems, and is a very important factor in modern warfare where communication systems and radars play a major role (Vakin et al. 2001). In particular, for systems widely used in most location-based weapon systems or commercial mobile communication systems such as global navigation satellite systems (GNSS), the effects of jamming are devastating. Interference signals intended to simply disturb reception are generally radiated at high power and are received by the receiver at a relatively higher power than normal information signals. However, GNSS signals are received at very low power, and thus even low-power interference signals have a significant effect (Borio et al. 2012).

Methods for detecting and mitigating interference in GNSS systems are categorized into antenna level techniques, automatic gain control (AGC) level techniques, post-correlation techniques, and processing techniques at the analog to digital converter (ADC) output (Musumeci & Dovis 2014). Antenna level techniques are generally based on the use of antenna arrays capable of generating radiation patterns to attenuate the interference.

In the case of AGC, we can monitor interference from the changes in the gain value because the AGC gain decreases when signals with large power are received. When there is interference, or when the AGC gain should be very small, the effect of interference is mitigated by maintaining the AGC gain at its normal value and thereby saturating the interference.

The processing methods of the ADC output include time-domain methods and frequency-domain methods. The time-domain methods monitor interference by detecting the energy change of signals during a fixed time window.

Received Nov 09, 2019 **Revised** Nov 22, 2019 **Accepted** Nov 25, 2019
†**Corresponding Author**
E-mail: boseok@cbnu.ac.kr
Tel: +82-43-261-3267 Fax: +82-504-315-4001

Bo-Seok Seo https://orcid.org/0000-0002-1610-3667
Kwi-Woo Park https://orcid.org/0000-0002-0338-2599
Chansik Park https://orcid.org/ 0000-0003-2650-4947

Interference signals are removed by applying the blanking method which sets the corresponding window section to 0. The frequency-domain method removes interference using inverse fast Fourier transform (IFFT) after filtering the frequency or band that includes the interference based on fast Fourier transform (FFT) of the signals.

The correlator calculates the correlation between the spreading code used by each satellite signal and the received signal. If there is no interference, the correlator output reveals a large peak at the time of code synchronization. However, the peak size becomes smaller if there is interference.

Recently, many methods using discrete wavelet transform (DWT) or discrete wavelet packet transform (DWPT) have been proposed for spectrum sensing and interference detection (Tian & Giannakis 2006, Divakaran et al. 2011, Choi et al. 2018, Dibal et al. 2018). DWPT gradually decomposes the signal into high-frequency and low-frequency bands by using wavelet and scaling functions. Therefore, we can adjust the transform level to have the desired frequency resolution because the bandwidth of the decomposed signal is reduced by 1/2 for each level of scale. Meanwhile, the time interval of the distinguishable signal increases as the level increases. As a result, methods using wavelet transform can change the resolution of time and frequency in contrast for each level, compared to FFT methods of fixed time and frequency resolution (Mallat 1989).

Divakaran et al. (2011) applied wavelet transform and energy detection methods to estimate spectrums for cognitive radios. Dibal et al. (2018) applied DWPT using Meyer wavelets to detect interference in GNSS signals and to mitigate the effects of interference. In each scale, the energy of the wavelet coefficients is compared with the threshold, and if the coefficient is greater than the threshold, it is set to 0. This method is applied to each step of scaling, and inverse DWPT (IDWPT) is used to obtain signals without interference.

The characteristics of wavelet transform, which divides bands into low-pass and high-pass bands, vary depending on the type of wavelet, resulting in different interference detection or interference mitigation capabilities. Based on the methods of Choi et al. (2018) and Divakaran et al. (2011), we apply DWPT to reduce the influence of interference in GPS L1 band C/A signals and compar the interference mitigation performance of 6 wavelets including Haar, Daubechies, Symlets, Coiflets, Biorthogonal Splines, and Discrete Meyer.

2. RECEIVED SIGNAL MODEL

GPS signals are received with noise from multiple satellites and can be expressed as Eq. (1) below.

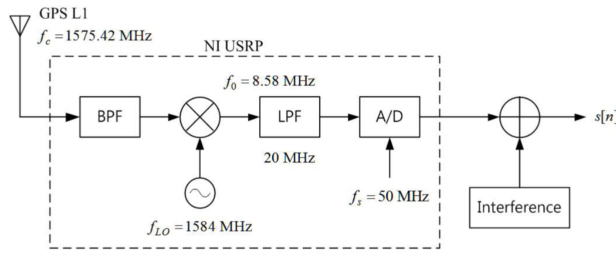

Fig. 1. Structure of the GPS receiver.

$$r(t) = \sum_{k \in S} s_k(t) + n(t) + i(t) \tag{1}$$

where $s_k(t)$ is k-th satellite signal, S is the set of satellite signal numbers received in a specific area among 32 GPS satellites, and $n(t)$ is the noise signal. The power of the received GPS signals is smaller than the noise power. Therefore, the spectrum of the signal is invisible due to noise. The interference $i(t)$, which is deliberately introduced to disturb the reception of signals, or unintentionally introduced at the same band.

In this paper, we use GPS L1 C/A signals that are actually received and interference signals that are simulated. In general, GPS L1 receivers apply intermediate frequency (IF) sampling techniques after lowering the center frequency of the signals to the IF band. The sampled signals undergo code synchronization, frequency synchronization, time synchronization, and demodulation by digital signal processing. In this paper, as shown in Fig. 1, we shift the center frequency of the GPS L1 signals to 8.58 MHz, limit the bandwidth to 20 MHz through a low-pass filter, and use the signals sampled at 50 MHz. The power spectral density (PSD) of the GPS signals received is very small compared to the PSD of noise. Thus, the spectrum of the sampled signals containing noise exists from 0 to 20 MHz. This process is performed using a USRP system from National Instruments.

The interference signals are software generated on a PC and added to the sampled GPS signals. The interference power is generally determined by the jamming to signal power ratio (JSR). In GPS signals, it is difficult to define the signal power because it is much smaller than the noise power due to spread-spectrum modulation, and because the signals from multiple satellites are received at different powers. In this paper, instead of JSR, we apply the jamming to noise power ratio (JNR), which is defined as the ratio of the interference power to the power of the received signal with noise in the GPS L1 C/A signal band, as shown in Eq. (2) below.

$$JNR \triangleq \frac{\text{Interference power}}{\text{Noise power in signal band}} \tag{2}$$

https://doi.org/10.11003/JPNT.2019.8.4.165

where the denominator can be expressed as the noise power because the signal power is much smaller than the noise power, and so the power of the received signal is almost equal to the noise power.

In actual GPS systems, the AGC is configured in front of the analog-to-digital (AD) converter to adjust the AGC gain so that the input of the AD converter is in the proper range. In this paper, we did not consider the effect of AGC gain changes because the interference signals are inserted after the AD converter.

3. INTERFERENCE DETECTION AND REMOVAL USING DWPT

3.1 Signal Decomposition using DWPT

DWT decomposes the input signal into low and high frequency components through scaling. This process is equivalent to passing the signal through low-pass and high-pass filters with bandwidth of 1/2 of the input signal band. The output of both filters can be expressed as Eqs. (3) and (4) below (Dibal et al. 2018).

$$y_H(n) = \sum_k x(k)\ h(2n-k) \tag{3}$$

$$y_L(n) = \sum_k x(k)\ g(2n-k) \tag{4}$$

where $y_H(t)$ and $y_L(t)$ are the outputs of the high-pass filter and low-pass filters, respectively, $h(n)$ and $g(n)$ are the scaling function and wavelet function in the wavelet transform, which represent the impulse response of the high-pass and low-pass filters. The two filter coefficients have the relationship shown in Eq. (5) (Mallat 1989).

$$g(n) = (-1)^n h(2k+1-n) \tag{5}$$

The frequency characteristics of filters vary depending on the type of wavelet. Fig. 2 shows the signal decomposition process using DWT and the input and output spectrum. In the figure, f_s is the sampling frequency of the discrete input signal.

If N is the number of DWT input samples, the number of samples of each output is $N/2$. As a result, for the sample time interval T_s of the input signal, the sample time interval of the DWT output becomes $2T_s$, thereby reducing the time resolution by 1/2. In other words, the output signal bandwidth is reduced to 1/2 of the input signal bandwidth, but shows twice the time interval in the time domain.

As shown in Fig. 3, DWPT repeatedly applies high-pass filter and low-pass filters to the 2 DWT output signals. Since

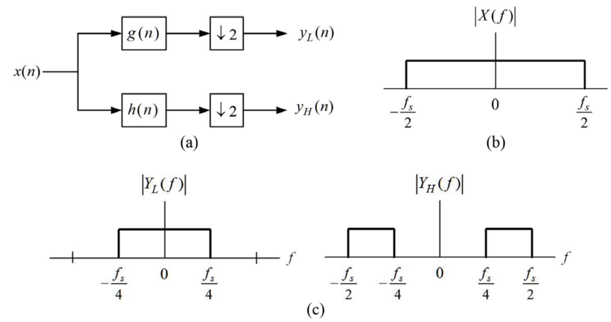

Fig. 2. Discrete wavelet transform. (a) Structure of highpass and lowpass filtering by DWT, (b) spectrum of input signal, and (c) spectrum of output signals

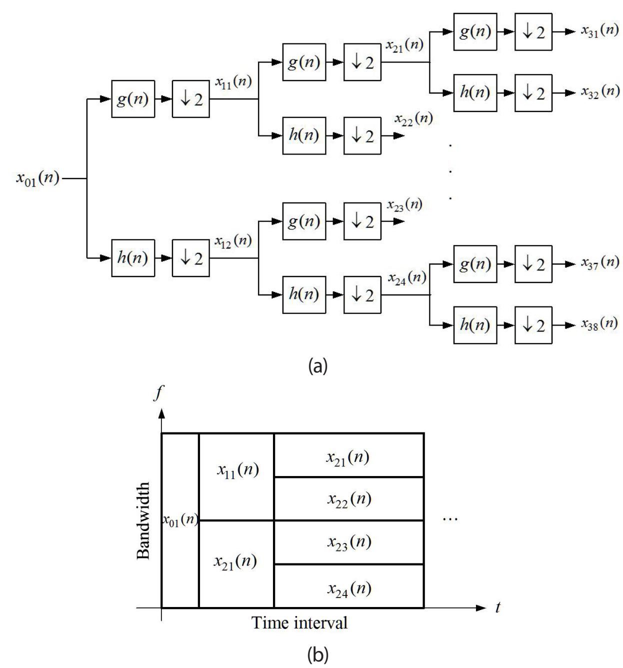

Fig. 3. Discrete wavelet packet decomposition. (a) Structure of DWPT, and (b) time-frequency characteristics of signals at different levels

the signal is repeatedly decomposed into high and low frequencies at each stage, it is divided into 2^M subband signals after M stages. The bandwidth of each output is reduced by $1/2^M$ and the sampling interval is increased by 2^M compared to the input signal. Therefore, considering the same number of samples, the bandwidth of the output at each step is reduced by 1/2 and the time interval is doubled compared to the input as shown in Fig. 3b.

The characteristics of DWT band decomposition vary depending on the type of wavelet. Fig. 4 shows the impulse response and spectrum of the 6 wavelet functions used in this paper — Haar, Daubechies, Symlets, Coiflets, Biorthogonal Splines, and Discrete Meyer, which are all fourth-order functions, except for the Haar wavelet. In the figure, the first 2 columns represent the scaling function $h(n)$ and the wavelet

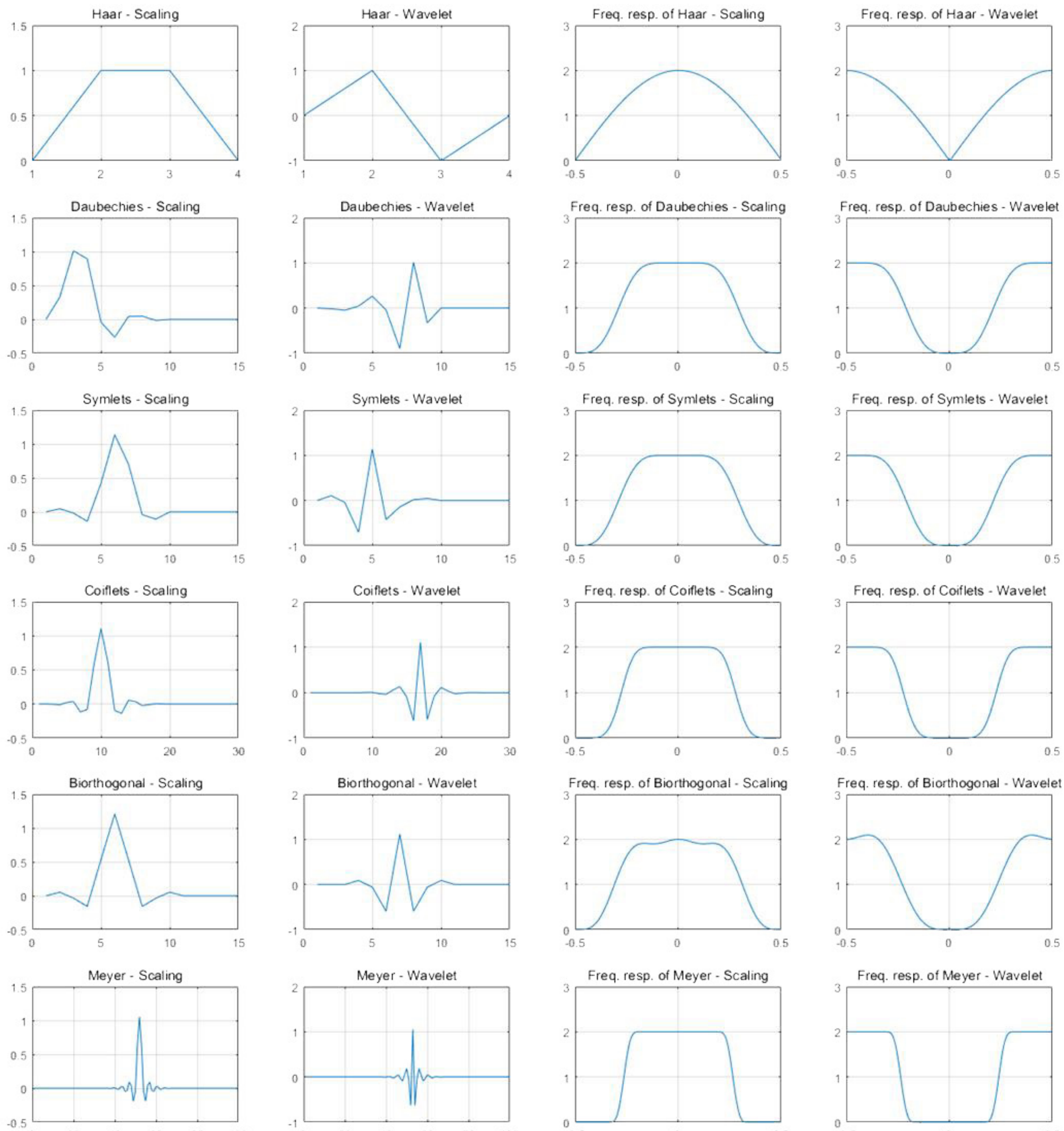

Fig. 4. Time and frequency responses of Haar, Daubechies, Symlets, Coiflets, Biorthogonal splines, and discrete Meyer wavelets.

function $g(n)$, respectively, and the latter 2 columns represent the corresponding frequency spectrums $|DFT[f(n)]|$ and $|DFT[g(n)]|$. The frequency spectrums are normalized from -0.5 to 0.5 for convenience.

3.2 Interference Detection and Removal using DWPT

When interference is introduced in a certain signal band, the output signal energy of the DWPT subband that includes the band increases. Because GPS signals are transmitted using a direct sequence spread spectrum method, even if a part of the signal is set to 0, the effect on the correlation with the spreading code is not critical if the length is much shorter than the length of the spreading code. If IDWPT is performed after setting the interference-detected DWPT subband output to 0, the sample with the value of 0 will be gradually

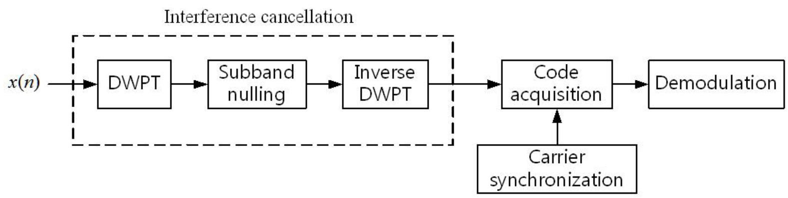

Fig. 5. Interference cancellation and demodulation in a GPS receiver.

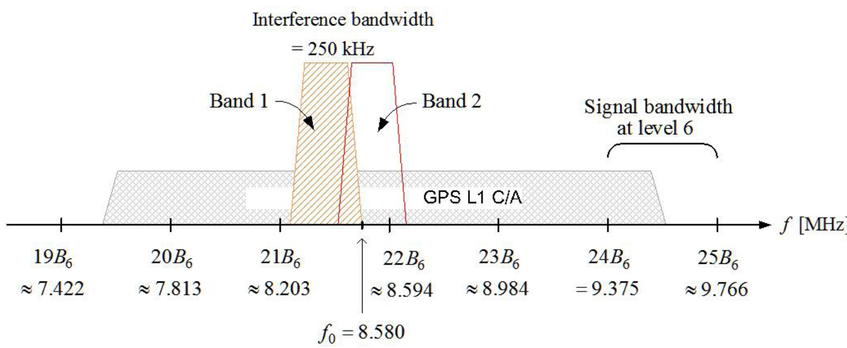

Fig. 6. Bands of GPS L1 C/A signal, interference, and DWPT outputs at level 6.

distanced due to double interpolation as the reconstruction stage proceeds reversely. Therefore, unless the interference is introduced in broadband, the effects can be mitigated in the despreading process.

Applying DWPT to detect and remove interference proceeds as follows.

(a) Signal decomposition

First, perform DWT on the sampled GPS L1 C/A signals with interference.

(b) Interference detection

Calculate the average power of the two DWT output signals as shown in Eq. (6).

$$P_{x(m,l)} = \frac{1}{N_{ml}} \sum_{n=1}^{N_{ml}} x_{ml}^2(n) \tag{6}$$

where x_{ml} is the l-th output signal of the m-stage of DWT and N_{ml} is the number of signal samples. If the number of samples of DWPT input is N_{01}, $N_{ml} = N_{01}/2^m$. If this average power is greater than the preconfigured threshold P_{th}, it is considered that interference is introduced. Then, the entire output is set to 0. Subband signals without interference go to step (a) for DWT again. Repeat steps (a) and (b) up to stage M.

(c) Original signal reconstruction

After repeating steps (a) - (b) for the subband signals without interference, perform IDWPT on the entire output to reconstruct the original signal.

(d) Perform demodulation by dispreading the reconstructed signal.

4. SIMULATION RESULTS

For the simulation, we used GPS L1 C/A signals that are received through a USRP system from National Instrument and sampled in the IF band. The interference signals which are frequency modulation (FM) signals generated by software are added to the IF band received signals. The FM signal is known to be effective for GPS jamming. As shown in Fig. 5, the signals with interference proceed to the demodulation process for detecting data using the spreading code and carrier synchronization after the interference mitigation process using DWPT. In this paper, we examine the interference mitigation performance from the correlation function between the input signal and the spreading code, which is obtained in the code and frequency synchronization process.

The sweep FM interference is modulated by triangular wave with bandwidth of 250 kHz and sweep time of 1 msec. We consider two cases for the interference band as shown in Fig. 6. The bandwidth of the 6-stage DWPT subband signal is B_6 = 25 MHz/2^6 = 390.625 kHz. Considering the IF band, Band 1 ranges from 8.33 MHz to 8.58 MHz which is the center frequency of GPS L1 signals, and the interference band is located within the subband of the DWPT output. Band 2 ranges from 8.39 MHz to 8.64 MHz across two 6-stage DWPT subbands.

According to the simulation results of this paper, the effect of the sweep FM interference becomes larger as the interference band narrows up to 250 kHz when the power is

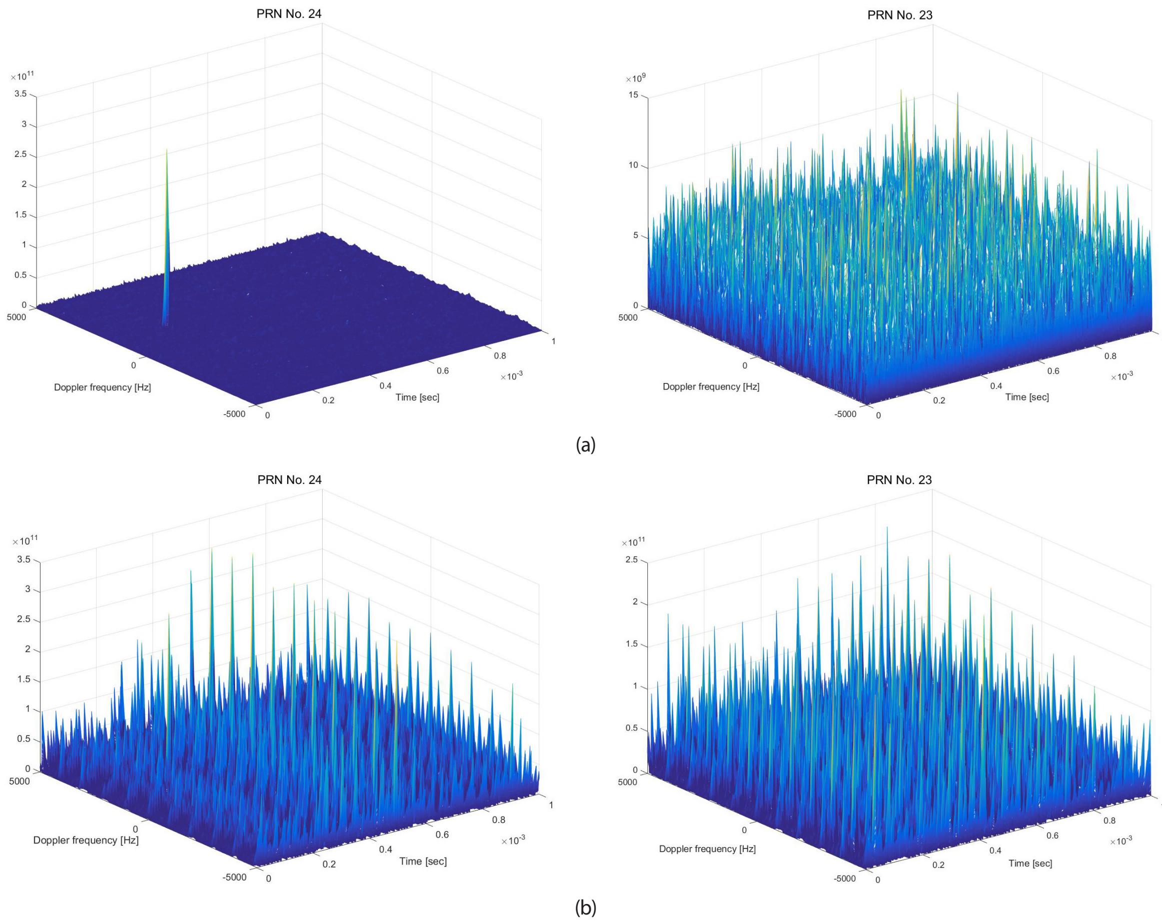

Fig. 7. Time-frequency plots of correlation functions of PRN number 24 and 23 spreading codes and received signals (a) without interference, and (b) with interference of 15 dB JNR.

the same. Below 250 kHz, the performance is almost the same in terms of peak ratio, so we fixed the interference bandwidth to 250 kHz.

Fig. 7 shows the correlation function in the time-frequency domain between the received signal and the pseudorandom noise (PRN) 24 and 23 spreading codes during 5 msec interval when there is no interference and when there is interference in Band 1. In the figure, the time axis represents time shift of the spreading code in the correlation operation, and the frequency axis indicates the difference from the center frequency of the GPS L1 signal. The PRN 24 signal is a signal from visible satellites and shows a clear peak, as shown in Fig. 7a, when there is no interference. The time and frequency at which this peak appears indicate the delay of the PRN 24 signal and the Doppler frequency shift caused by the relative moving between the satellite and the receive antenna. This value is used to synchronize with the spreading code during the dispreading process and applied to carrier synchronization for data detection. The PRN 23 signal in Fig. 7a shows the correlation function of signals from invisible satellites, and the satellite signal cannot be obtained because there is no distinct peak. Fig. 7b presents the correlation functions of the PRN 24 and 23 when the JNR is 15 dB, and in this case, satellite signals cannot be obtained as well.

In general, the obtained satellite signals may also have more than one peak in the correlation function due to multipath transmission channel. This may result in errors in the maximum peak position due to external interference or noise. We define the peak ratio of correlation values as shown in Eq. (7) as a measure of interference mitigation performance.

$$Peak\ ratio = \frac{\text{Correlation value at the first peak}}{\text{Correlation value at the second peak}} \qquad (7)$$

We consider that code synchronization has been achieved only if this peak ratio is greater than a certain threshold, and then proceed to the next steps. The peak ratio threshold ranges from 2 to 3.

The peak ratio with 32 PRN codes when interference exists in Band 1 is shown in Fig. 8. The peak ratio is obtained by

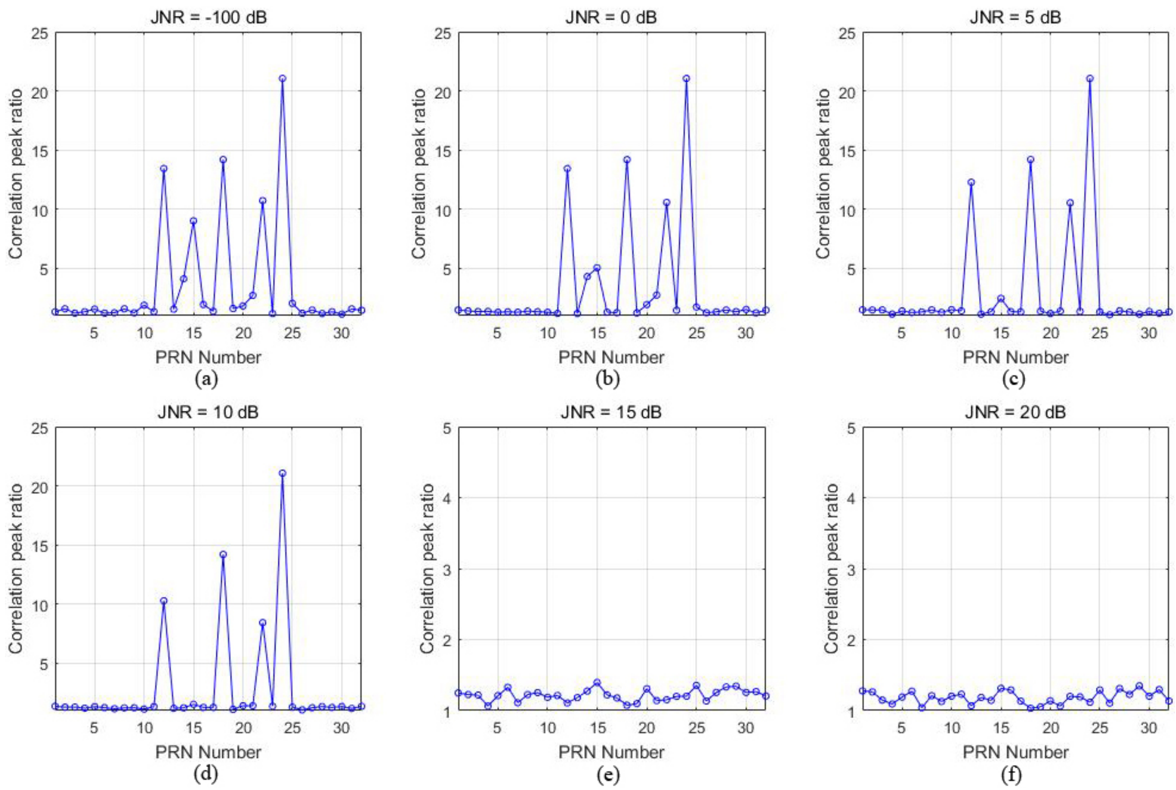

Fig. 8. Peak ratios for 32 PRN codes with different JNRs of (a) -100 dB (almost no interference), (b) 0 dB, (c) 5 dB, (d) 10 dB, (e) 15 dB, and (f) 20 dB.

averaging the results of 20 independent simulations. When the JNR is -100 dB, there is almost no interference because the interference power is very small. As shown in the figure, with a peak ratio threshold of 2, the number of acquisitions remains the same although the peak ratio for some PRN codes is reduced at 0 dB of JNR. However, the number of satellite signals acquired begins to decrease from 5 dB of JNR, and almost no satellite signals can be acquired when the JNR is above 15 dB.

Fig. 9 shows the peak ratio when interference is detected and mitigated by applying DWPT with 6 wavelets. Each DWPT is applied up to 6 levels. The threshold of the average power to detect interference is set empirically to 3 times the average power of the entire signals through simulations. The figure shows that satellite signals can be obtained up to about 40 dB of JNR, depending on the type of the wavelet.

Fig. 10 shows the number of acquired signals with JNR, assuming that satellite signals can be acquired when the peak ratio is greater than 2. The figure shows that more satellite signals can be obtained when applying Coiflets and discrete Meyer wavelets. As seen from Fig. 4, this is because the amplitude spectrum of the two wavelets is sharper in the transition band than the others. When interference is introduced into a certain subband, the signals of the subband are all set to 0 and then reconstructed to remove the interference which has larger amplitudes than the signals. If the amplitude characteristics of the filter are not sharp, only a part of the interference is removed near the boundary of the adjacent two subbands, and the desired signals of adjacent subband are suppressed, which in turn affects the performance. Among the frequency characteristics of the wavelets, however, phase linearity does not seem to have a significant effect on the performance. The amplitude characteristics of Daubechies and Symlets wavelets are almost the same, but the Symlet wavelet is of linear phase and the Daubechies wavelet is of nonlinear phase. The figure shows that the performance of the two wavelets is almost the same.

Fig. 11 shows the number of signals acquired with JNR when the interference band is Band 2. Compared to Fig. 10, we can see that satellite signals can be obtained even at 45 dB of JNR. Also, the number of signals acquired at the same JNR increased for all of the wavelets, except for Haar. This is considered as a result of the interference power being divided into two bands, which leads to a relative reduction in interference power. However, as in the case of Fig. 10, Coiflets and discrete Meyer wavelets show better performance than the others.

5. CONCLUSION

In this paper, we apply DWPT to reduce the influence of

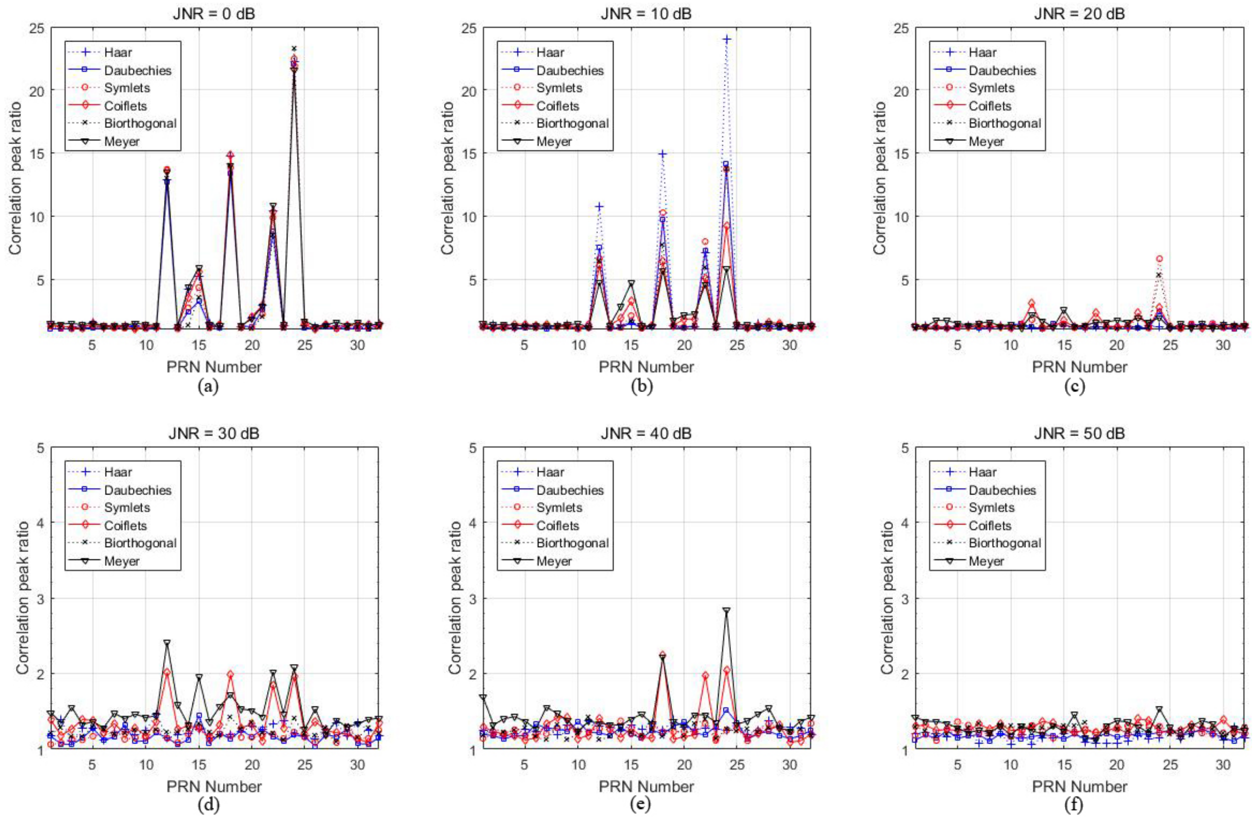

Fig. 9. Peak ratios when DWPT and interference cancellation is applied with 6 wavelets for different JNRs of (a) -100 dB (almost no interference), (b) 0 dB, (c) 10 dB, (d) 20 dB, (e) 30 dB, 40 dB, and (f) 50 dB.

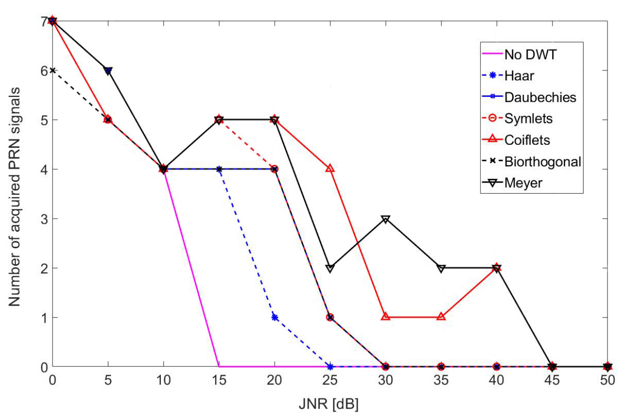

Fig. 10. Number of satellite signals captured for interference band 1.

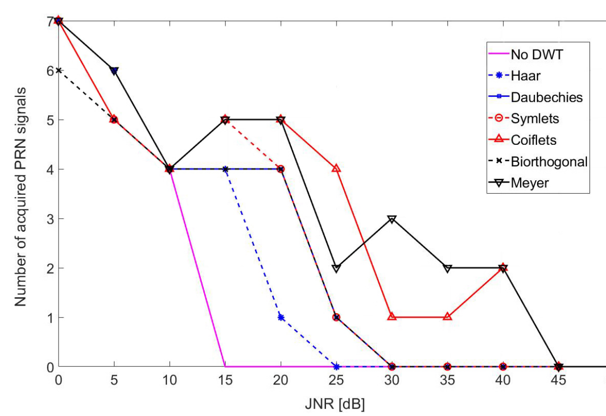

Fig. 11. Number of satellite signals captured for interference band 2.

interference in GPS L1 band C/A signals and compare the interference mitigation performance of 6 wavelets—Haar, Daubechies, Symlets, Coiflets, Biorthogonal Splines, and Discrete Meyer. In the case where interference is sweep FM with 1 msec of sweep time and 250 kHz of bandwidth, simulation results show that the Coiflets and discrete Meyer wavelets yield better performance. The Daubechies wavelet and Symlets wavelet, which have similar amplitude characteristics but different phase linearity characteristics in frequency characteristics of wavelet functions, show almost the same performance. These results suggest that the interference mitigation performance of DWPT with interference of sweep FM is mainly determined by the amplitude characteristics of wavelets and that phase linearity does not have a significant effect on performance.

In the simulation, decomposition and reconstruction by using wavelets or wavelet transform and inverse wavelet transform are performed in block-wise. However, wavelet transform corresponds to filtering, thus real-time processing is possible through continuous decomposition and reconstruction. Meanwhile, even if there is interference in the same bandwidth, the interference mitigation performance slightly varies depending on the position in the DWPT subband. Further research is required for real-time processing, on the influence of the position of the interference band, and on the effects of system imperfections in frequency and time synchronization, in the future.

AUTHOR CONTRIBUTIONS

Conceptualization, B. S. Seo, K. W. Park, C. Park; methodology, B. S. Seo, K. W. Park, C. Park; software, B. S. Seo, K. W. Park, C. Park; validation, B. S. Seo; formal analysis, B. S. Seo; writing—original draft preparation, B. S. Seo; writing—review and editing, B. S. Seo; visualization, B. S. Seo.

CONFLICTS OF INTEREST

The authors declare no conflict of interest.

REFERENCES

Borio, D., O'Driscoll, C., & Fortuny, J. 2012, GNSS Jammers: Effects and countermeasures, in 2012 6th ESA Workshop on Satellite Navigation Technologies (Navitec 2012) & European Workshop on GNSS Signals and Signal Processing, 5-7 Dec 2012, Noordwijk, Netherlands. https://doi.org/10.1109/NAVITEC.2012.6423048

Choi, J. W., Hong, S. J., Park, C., & Seo, B. S. 2018, Wideband interference detection by using discrete wavelet transform in a direct RF sampling receiver, Proc. of International Conference on Electronics, Information and Communication (ICEIC), Hawaii, USA, 24-27 Jan. 2018, pp.1241-1242

Dibal, P. Y., Onwuka, E. N., Agajo, J., & Alenoghena, C. O. 2018, Application of wavelet transform in spectrum sensing for cognitive radio - a survey, Physical Communication, 28, 45-57. https://doi.org/10.1016/j.phycom.2018.03.004

Divakaran, K., Manikandan, P, N., & Hari, R. R. S. 2011, Wavelet based spectrum sensing techniques for cognitive radio - Survey, International Journal of Computer Science & Information Technology (IJCSIT), 3, 123-124. https:/doi.org/10.5121/ijcsit.2011.3209

Mallat, S. G. 1989, A Theory for Multiresolution Signal Decomposition: The Wavelet Representation, IEEE Trans. on Pattern Analysis and Machine Intelligence, 11, 674-693. https://doi.org/10.1109/34.192463

Musumeci, L. & Dovis, F. 2014, Use of the wavelet transform for interference detection and mitigation in global navigation satellite systems, International Journal of Navigation and Observation, 2014, Article ID 262186. https://doi.org/10.1155/2014/262186

Tian, Z. & Giannakis, G. B. 2006, A wavelet approach to wideband spectrum sensing for cognitive radios, 2006 1st International Conference on Cognitive Radio Oriented Wireless Networks and Communications, Mykonos Island, Greece, 8-10 June 2006, https://doi.org/10.1109/CROWNCOM.2006.363459

Vakin, S. A., Shustov, L. N., & Dunwell, R. H. 2001, Fundamentals of Electronic Warfare (Boston, London: Artech House)

Bo-Seok Seo received B.S., M.S., and Ph.D. degrees in electronics engineering from Seoul National University, Korea, in 1987, 1989, and 1997, respectively. He is currently a professor in Department of Electronics Engineering, Chungbuk National University. His research interests include GNSS signal processing and wireless communication systems.

Kwi-Woo Park received his B.S., M.S., and Ph.D. degrees from Chungbuk National University, Korea in 2013, 2015, and 2019, respectively. He is currently an associate research engineer of Navcours Co, Ltd. His research interests include GNSS, TWSTFT, eLoran signal processing and software defined radio.

Chansik Park received his B.S., M.S., and Ph.D. degrees in Electrical Engineering from Seoul National University in 1984, 1986 and 1997, respectively. He is currently a professor in Department of Electronics Engineering, Chungbuk National University, Cheongju, Korea, since 1997. His research interests include GNSS, PNS, SDR, integer ambiguity resolution algorithm and Error Analysis.